Available online at www.sciencedirect.com
ScienceDirect
Radiation Measurements 41 (2006) 1142–1146
Radiation Measurements
www.elsevier.com/locate/radmeas

Applicability of particle and heavy ion transport code PHITS to the shielding design of spacecrafts

Tatsuhiko Sato[a,*], Koji Niita[b], Hiroshi Iwase[c], Hiroshi Nakashima[a], Yasuhiro Yamaguchi[a], Lembit Sihver[d,e]

[a]*Research Group for Radiation Protection, Division of Environment and Radiation Sciences, Nuclear Science and Engineering Directorate, Japan Atomic Energy Agency (JAEA), Shirakata-Shirane 2-4, Tokai, Naka, Ibaraki, 319-1195, Japan*
[b]*Research Organization for Information Science and Technology (RIST), Japan*
[c]*GSI, Germany*
[d]*Chalmers University of Technology, Sweden*
[e]*Roanoke College, USA*

Received 2 April 2006; received in revised form 30 April 2006; accepted 2 July 2006

Abstract

Development of HZE particle transport codes is severely required for the shielding design of spacecrafts. One-dimensional deterministic codes are generally adopted in the shielding calculation because of their reasonable computational time, but three-dimensional Monte Carlo codes are also to be employed especially in the final step of the design with fully optimized geometries. We are therefore developing a general-purpose Monte Carlo code PHITS, which can deal with the transports of all kinds of hadrons and heavy ions with energies up to 200 GeV/n. For the purpose of examining the applicability of PHITS to the shielding design, neutron and charged particle spectra inside the Space Shuttle were calculated for an imaginary vessel whose shielding distribution is fitted to that of the real shuttle. Absorbed doses and dose equivalents were estimated from the spectra by applying fluence to dose conversion coefficients. The agreements between the calculated spectra or doses and the corresponding experimental data were generally satisfactory, especially for the neutron spectra, which have been barely reproduced by other studies. We therefore concluded that PHITS has a great possibility of playing an important role in the design study of spacecrafts.

1. Introduction

Evaluation of doses for astronauts has been an essential issue in the planning of long-term space missions. The prime attention has been paid to evaluating doses from primary cosmic rays directly incident to astronauts, but the estimation of doses from secondary particles, especially neutrons, is also of great importance because of their large contribution to the total doses—60% at the maximum (Badhwar et al., 2001). Development of hadron and heavy ion transport codes is therefore required in the design study of spacecrafts, since a variety of heavy ions as well as protons can be the sources of the secondary particles by causing nuclear reactions inside the shielding materials. One-dimensional deterministic codes are generally adopted in the shielding calculation owing to their reasonable computational time, but three-dimensional Monte Carlo codes are also to be employed especially in the final step of the design with fully optimized geometries (Wilson et al., 2002).

We are therefore developing a general-purpose Monte Carlo code PHITS (Iwase et al., 2002) (Particle and Heavy Ion Transport code system), which can deal with the transports of all kinds of hadrons and heavy ions with energies up to 200 GeV/n. PHITS is based on the high energy hadron transport code NMTC/JAM (Niita et al., 2001), and incorporates the MCNP4C code (Briesmeister, 1997) for low energy neutron transports and the JAERI quantum molecular dynamics (JQMD) model (Niita et al., 1995) for simulating nucleus–nucleus interactions.

* Corresponding author. Tel.: +81 29 282 5803; fax: +81 29 282 6768.
E-mail address: sato.tatsuhiko@jaea.go.jp (T. Sato).

1350-4487/$ - see front matter © 2006 Elsevier Ltd. All rights reserved.
doi:10.1016/j.radmeas.2006.07.014

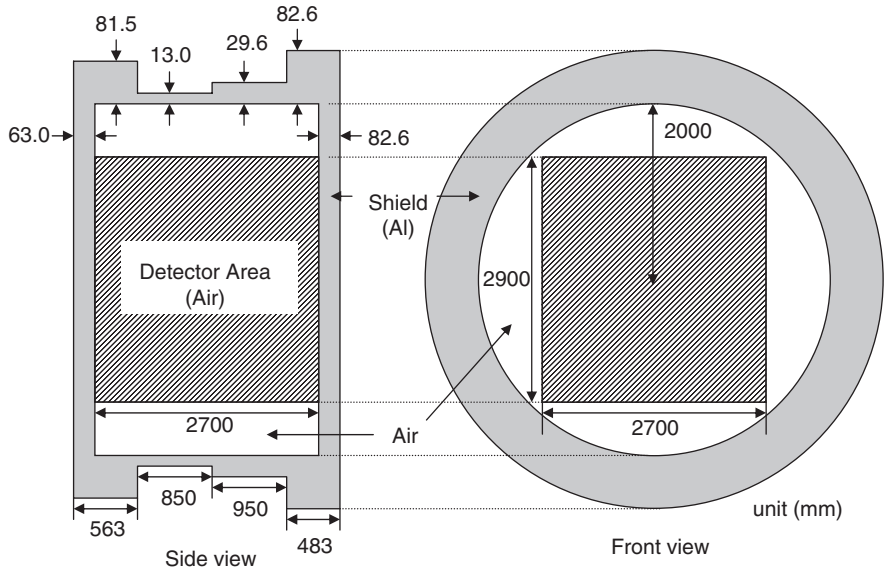

Fig. 1. Structure of the imaginary vessel—the substitution for the Space Shuttle with the SPACEHAB module in our simulation.

A detail about the recent development of the code is given in elsewhere on this issue.[1]

For the purpose of examining the applicability of PHITS to the shielding design, neutron and charged particle spectra inside the Space Shuttle were calculated by assuming the vehicle as an imaginary vessel whose shielding distribution is fitted to that of the real shuttle. Absorbed doses and dose equivalents were estimated from the spectra by applying fluence to dose conversion coefficients. A detailed description of the simulation procedure is presented below, together with some comparisons between the calculations and experiments.

2. Calculation method

2.1. Geometry

The simulations to estimate the particle spectra inside spacecrafts were performed for reproducing the flight conditions of STS-89 and STS-91, in which the measurements of neutron spectra with Bonner ball neutron detector (BBND) (Matsumoto et al., 2001) and absorbed doses with thermoluminescent dosimeters (TLD) in a human phantom (Badhwar et al., 2002; Yasuda et al., 2000) were carried out, respectively. The phantom and BBND were mounted in the SPACEHAB module loaded on the shuttle. However, detailed structures of the module as well as the shuttle are generally not available. An imaginary aluminum vessel was therefore substituted for the shuttle with the module in our simulation. The averaged shielding distribution inside the vessel is fitted to those at the locations of the tissue-equivalent proportional counter (TEPC) and the charged-particle directional spectrometer (CPDS), which were also mounted in the module at the STS-91 flight.

Fig. 1 illustrates the structure of the imaginary vessel. The differential and cumulative shielding distributions averaged over the detector area are shown in Fig. 2, together with those at the locations of the TEPC and CPDS shown in Badhwar et al. (2002). It can be seen in Fig. 2 that both of the shielding distributions agree with the corresponding data very well. It should be noted that the shielding distributions at the locations of the human phantom and BBND, which are to be reproduced in our simulation, differ from those of the TEPC and CPDS, since the distribution depends on the detailed positions where the detectors were mounted in SPACEHAB.

To analyze the shielding material and thickness dependences of doses for astronauts in spacecrafts, particle spectra inside simple cylindrical shells made of aluminum and PMMA were also calculated by changing their thicknesses from 0 to 80 g/cm^2. The length and inner radius of the shell are the same as those of the imaginary vessel depicted in Fig. 1.

2.2. Source particle

In our simulation, the vessels were irradiated in the radiation field in the orbit of 380 km altitude and 51.6° inclination at the solar minimum, which represents the flight conditions of STS-89 and STS-91. Similar simulations were also performed for the solar maximum condition in the same orbit.

Almost all kinds of space radiations—the trapped and Galactic Cosmic Ray (GCR) protons, albedo neutrons from the earth atmosphere, and heavy ions with charges up to 28 and energies up to 100 GeV/n—were considered as the source particles in the calculation. The CREME96 code (Tylka et al., 1997) was adopted for the estimation of the charged particle

[1] K. Niita, T. Sato, H. Iwase, H. Nakashima, L. Sihver, Particle and heavy ion transport code system: PHITS, on this issue.

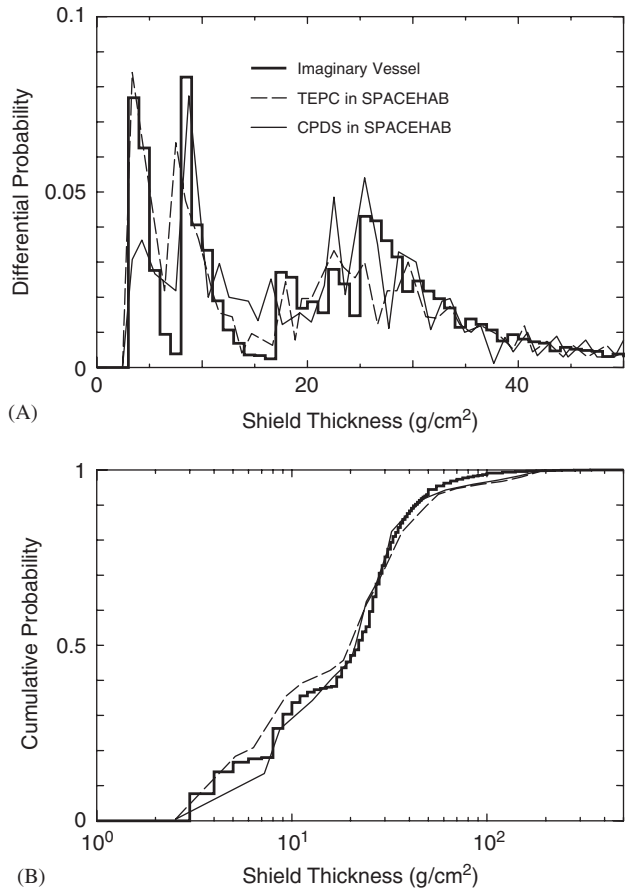

Fig. 2. Differential (A) and Cumulative (B) shielding distributions averaged over the detector area in the imaginary vessel, together with those at the locations of the TEPC and CPDS flown in STS-91.

spectra outside the vessels. The spectrum of albedo neutrons was obtained from the simulation of particle transport in the earth atmosphere performed by PHITS, in which charged particles with the spectra at 86 km altitude were employed as the source particles. The detailed of the calculation procedure for the estimation of the albedo neutron spectrum is described in Sato and Niita (2006).

2.3. Dose estimation

Absorbed doses and dose equivalents in bone marrow, stomach and skin were estimated from the particle spectra in the vessels by applying fluence to dose conversion coefficients for the isotropic irradiation geometry. Absorbed doses for whole body D_E and effective dose equivalents H_E—weighted sums of those in some organs and tissues specified in ICRP60 (1991)—were also calculated. The conversion coefficients adopted in the calculation were computed by PHITS with an anthropomorphic phantom by employing the tissue weighting factors and Q–L relationship defined in ICRP60. Some of them have been published in Sato et al. (2003a,b, 2004) and the others will be released in the near future. The exposure fluctuations of astronauts due to orientation (Wilson et al., 1993) were not taken into account, but the assumption of the isotropic irradiation was fairly adequate for our calculation, since the shielding thickness for each direction is not reproduced by our simulation. It should be noted that the use of the ambient dose equivalent $H^*(10)$, which generally gives a conservative estimation of the effective dose equivalent, is hardly adequate in the dose evaluation for astronauts, since it requires much higher precision than that for the public or workers in nuclear facilities does.

3. Results and discussion

3.1. Neutron spectrum

Fig. 3 shows the comparison of the calculated neutron spectrum in the imaginary vessel at the solar minimum with the orbit-averaged data measured by BBND at STS-89 (Matsumoto et al., 2001). The statistical uncertainties in the calculation

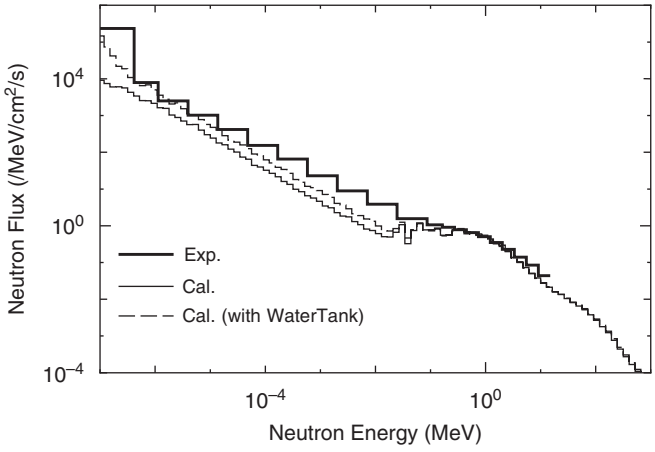

Fig. 3. Comparisons of the calculated neutron spectra in the imaginary vessel at the solar minimum with the orbit-averaged data measured by BBND at STS-89 (Matsumoto et al., 2001).

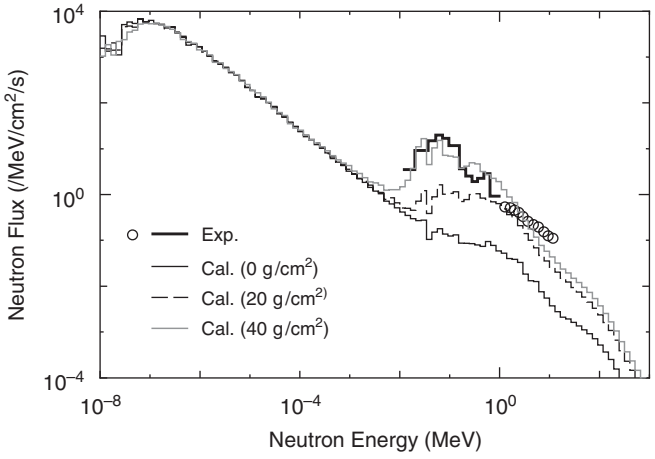

Fig. 4. Neutron spectra inside the aluminum cylindrical shells with different thicknesses at the solar maximum. Experimental data measured in the MIR space station with 40 g/cm^2 shielding (Dudkin et al., 1996) are also shown in this figure.

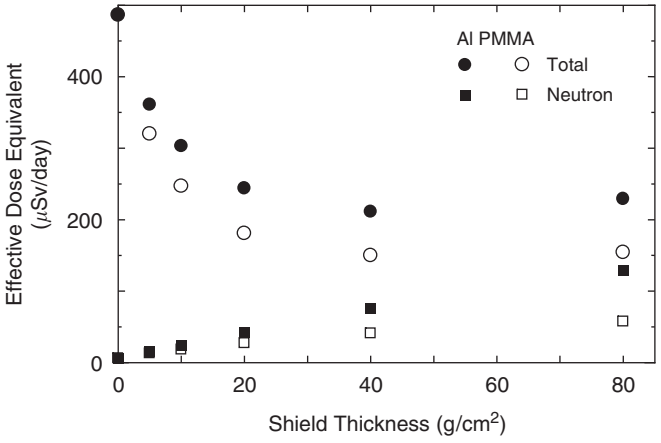

Fig. 5. Calculated effective dose equivalents for an astronaut staying in simple cylindrical shells made of aluminum and PMMA with different thicknesses at the solar maximum. Neutron contributions to the values are also shown in this figure.

are negligibly small. The calculated and experimental data are in close agreement for neutron energies above 0.1 MeV—the energy region of importance from the viewpoint of dose evaluation. On the other hand, the calculation generally underestimates the neutron fluxes below the energy. This discrepancy is probably attributed to the existence of a water tank near BBND. For estimating the effect of the water tank on the spectrum, we performed a similar simulation but placing 1 m^3 of water at the center of the imaginary vessel. The calculated neutron spectrum in the vessel with the water tank is also depicted in Fig. 3. It is evident from the graph that the existence of water increases the low energy neutron fluxes, and the values become closer to the experimental data.

Fig. 4 illustrates the shielding thickness dependence of the neutron spectra inside the aluminum cylindrical shells at the solar maximum. The yields of neutrons below 10 keV are almost independent of the thickness. Those above the energy, on the other hand, increase consistently with the thickness. This is because almost all neutrons below the energy originate from the earth albedo, while locally produced neutrons have the primary contribution to the total yields for the higher energies. The neutron spectra measured in the MIR space station with 40 g/cm^2 shielding (Dudkin et al., 1996) are also plotted in Fig. 4. The calculated spectrum for the corresponding thickness agrees with the experimental data fairly well, although the structure of the spacecraft was simply assumed as the cylindrical shell in the simulation.

3.2. Neutron dose

Table 1 gives the comparisons of the calculated neutron dose rates with the experimental data at STS-89 (Matsumoto et al., 2001). The agreements are generally satisfactory, though slight underestimations by the calculation are observed. These discrepancies may be attributed to the difference between the structures of the imaginary vessel and the real spacecraft. The ignorance of objects around the detector such as the water tank in the calculation can also cause the underestimation, especially for doses from lower energy neutrons. The calculation also indicates that more than a half of the total doses are due to neutrons with energies above 15 MeV. Hence, measurement of the higher energy neutron spectrum is indispensable for the precise evaluation of the total neutron doses.

3.3. Dose from all particles

Table 2 shows the calculated and experimental dose rates (Badhwar et al., 2002; Yasuda et al., 2000) for bone marrow, stomach and skin in the human phantom mounted on STS-91. The calculated absorbed doses for whole body and effective dose equivalents are also reported in the table. Our calculation indicates that the dose equivalent in bone marrow is almost equal to the effective dose equivalent and about 20% smaller than that in skin.

The calculated values generally agree with experimental data fairly well except for those in stomach, where the model predictions are substantially below the measured values. This underestimation may be induced by the ignorance of the anisotropic irradiation effect in our simulation, since the doses in stomach are significantly influenced by the distribution of the incident particle directions to the body. The doses in bone marrow and skin are not so affected by the anisotropy because of their overall distribution in the whole body.

Fig. 5 shows the shielding material and thickness dependences of the calculated effective dose equivalent for the solar maximum condition. The contributions of neutron to the values are also depicted in the graph. It is evident from the figure that the total effective dose equivalents decrease with an increase of the shielding thickness up to 40 g/cm^2. The values, however, remain almost constant for the thicker shielding case, since the

Table 1
Comparison between calculated and experimental neutron dose rates (Matsumoto et al., 2001) in the SPACEHAB module mounted on STS-89

Energy range	Below 0.1 MeV		0.1–1.0 MeV		1.0–15 MeV		Above 15 MeV	
	Cal.[a]	Exp.[b]	Cal.[a]	Exp.[b]	Cal[a]	Exp.[b]	Cal.[a]	Exp.[b]
D_E (μGy/day)	0.0150	0.0530	0.174	0.182	1.67	2.46	7.92	—
H_E (μSv/day)	0.0433	0.125	1.59	1.65	15.9	22.4	26.3	—

[a]The calculated values were estimated from the neutron spectrum inside the imaginary vessel at the solar minimum.
[b]The experimental values were obtained from the orbit-averaged neutron spectrum by applying the same dose conversion coefficients adopted in the derivation of the calculated doses.

Table 2
Comparison between calculated and experimental dose rates (Badhwar et al., 2002; Yasuda et al., 2000) at the locations of bone marrow, stomach and skin of a human phantom mounted on STS-91

	PHITS[a]		Measured data[b]		
	Absorbed dose (μGy/day)	Dose equivalent (μSv/day)	Absorbed dose (μGy/day)		Dose equivalent (μSv/day)
			NASA	NASDA	
Bone marrow	146	330	179 ± 13	184 ± 10	347 ± 41
Stomach	138	330	209 ± 23	245 ± 31	439 ± 51
Skin	210	430	245 ± 6.7	230 ± 42	459 ± 7.2
D_E and H_E	151	339			

[a]The calculated values were estimated from the particle spectra inside the imaginary vessel at the solar minimum.
[b]The experimental values were obtained from the total doses measured by TLDs, which are given in Table 1 of Badhwar et al. (2002), divided by the flight duration. The data for skin are the averaged values of the doses in skin/breast and skin/abdomen.

effects of secondary particles such as neutron become larger with a rise of the shielding thickness. The figure also indicates that PMMA is superior to aluminum in terms of the dose reduction rate. This is because PMMA can suppress the increase of secondary particle doses because of its smaller cross sections of fragmentation reactions. Note that these tendencies were also observed in the measurement by TEPC mounted on the Space Shuttle (Badhwar and Cucinotta, 2000).

4. Conclusion

The applicability of PHITS to the shielding design of spacecrafts was examined by comparing calculated neutron spectra and doses for astronauts in the Space Shuttle with the corresponding experimental data. The agreements between the data were generally satisfactory, especially for the neutron spectra, which have been barely reproduced by other studies. We therefore concluded that PHITS has a great possibility of being an indispensable implement in the design study of spacecrafts.

Acknowledgments

The authors wish to thank Dr. J.W. Wilson and Dr. H. Matsumoto for their helpful advices on this work.

References

Badhwar, G.D., Cucinotta, F.A., 2000. A comparison of depth dependence of dose and linear energy transfer spectra in aluminum and polyethylene. Radiat. Res. 153, 1–8.

Badhwar, G.D., Keith, J.E., Cleghorn, T.F., 2001. Neutron measurements onboard the space shuttle. Radiat. Meas. 33, 235–241.

Badhwar, G.D., Atwell, W., Badavi, F.F., Yang, T.C., Cleghorn, T.F., 2002. Space radiation absorbed dose distribution in a human phantom. Radiat. Res. 157, 76–91.

Briesmeister, J.F., 1997. MCNP—a general Monte Carlo *n*-particle transport code. LA-12625-M, Los Alamos National Laboratory, Los Alamos, NM.

Dudkin, V.E., Potapov, Yu.V., Akopova, A.B., Melkumyan, L.V., Bogdanov, V.G., Zacharov, V.I., Plyuschev, V.A., Lorabakov, A.P., Lyagushin, V.I., 1996. Measurements of fast and intermediate neutron energy spectra on Mir space station in the second half of 1991. Radiat. Meas. 26 (3), 535–539.

International Commission on Radiological Protection, 1991. 1990 recommendations of the International Commission on Radiological Protection. ICRP Publication 60, Ann. ICRP 21(1–3), Pergamon Press, Oxford.

Iwase, H., Niita, K., Nakamura, T., 2002. Development of a general-purpose particle and heavy ion transport Monte Carlo code. J. Nucl. Sci. Technol. 39 (11), 1142–1151.

Matsumoto, H., Goka, T., Koga, K., Iwai, S., Uehara, T., Sato, O., Takagi, S., 2001. Real-time measurement of low-energy-range neutron spectra on board the space shuttle STS-89 (S/MM-8). Radiat. Meas. 33, 321–333.

Niita, K., Chiba, S., Maruyama, T., Takada, H., Fukahori, T., Nakahara, Y., Iwamoto, A., 1995. Analysis of the (N, xN') reactions by quantum molecular dynamics plus statistical decay model. Phys. Rev. C52, 2620.

Niita, K., Meigo, S., Takada, H., Ikeda, Y., 2001. High energy particle transport code NMTC/JAM. JAERI-Data/Code 2001-007, Japan Atomic Energy Research Institute, Ibaraki, Japan. 2001.

Sato, T., Niita, K., 2006. Analytical functions to predict cosmic-ray neutron spectra in the atmosphere. Radiat. Res. 166, 544–555.

Sato, T., Tsuda, S., Sakamoto, Y., Yamaguchi, Y., Niita, K., 2003a. Analysis of dose-LET distribution in the human body irradiated by high energy hadrons. Radiat. Prot. Dosim. 106 (2), 145–153.

Sato, T., Tsuda, S., Sakamoto, Y., Yamaguchi, Y., Niita, K., 2003b. Conversion coefficients from fluence to effective dose for heavy ions with energies up to 3 GeV/*A*. Radiat. Prot. Dosim. 106 (2), 137–144.

Sato, T., Tsuda, S., Sakamoto, Y., Yamaguchi, Y., Niita, K., 2004. Profile of Energy Deposition in Human Body Irradiated by Heavy Ions. J. Nucl. Sci. Technol. Suppl. 4, 287–290.

Tylka, A.J., Adams Jr., J.H., Boberg, P.R., Brownstein, B., Dietrich, W.F., Flueckiger, E.O., Petersen, E.L., Shea, M.A., Smart, D.F., Smith, E.C., 1997. CREME96: a revision of the cosmic ray effects on micro-electronics code. IEEE Transactions on Nuclear Science 44, 2150–2160.

Wilson, J.W., Nealy, J.E., Wood, J.S., Qualls, G., Atwell, W., Shinn, J.L., Simonsen, L.C., 1993. Exposure fluctuations of astronauts due to orientation. NASA TP-3364, NASA Langley Research Center, Hampton, VA, 1993.

Wilson, J.W., Tripathi, R.K., Qualls, G.D., Cucinotta, F.A., Prael, R.E., Norbury, J.W., Heinbockel, J.H., Tweed, J., Angelis, G.D., 2002. Advances in space radiation shielding codes. J. Radiat. Res. 43 (Suppl.), 87–91.

Yasuda, H., Badhwar, G.D., Komiyama, T., Fujitaka, K., 2000. Effective dose equivalent on the ninth Shuttle-Mir mission (STS-91). Radiat. Res. 154, 705–713.